Advanced Electrochemical Characterization of Copper Deposition

by

Mary Elizabeth Wagner

Submitted to the Department of Materials Science and Engineering

In Partial Fulfillment of the Requirements for the Degree of

Bachelor of Science

at the

Massachusetts Institute of Technology

June 2016

Signature of Author……

Mary Elizabeth Wagner

Department of Materials Science and Engineering

May 2015

Certified by……

Antoine Allanore

Thomas B. King Assistant Professor of Metallurgy

Thesis Supervisor

Accepted by……

Geoffrey Beach

Associate Professor of Materials Science and Engineering

Chairman of the Undergraduate Committee

Abstract

The electrodeposition of copper metal in a concentrated sulfuric acid solution is reported to occur through a four-step mechanism: (I) the dehydration of $Cu^{2+}(H_2O)_6$, (II) the reduction of Cu^{2+} to Cu^{+}, (III) the dehydration $Cu^{+}(H_2O)_{6-x}$, (IV) the reduction of Cu^{+} to copper metal. The dehydration steps have been found to be responsible for the pH-dependence of the electrodeposition reaction. It is also reported, although not well understood, that the presence of Fe^{2+} ions affects the reaction kinetics. In this work, the kinetics of copper electrodeposition were studied using alternating current cyclic voltammetry. The reaction was studied at a copper rotating disk electrode with varying concentrations of Cu^{2+} and Fe^{2+}. At sufficiently low pH, and a sufficiently high concentration of Fe^{2+}, the deposition kinetics may be slowed enough to separately observe the two electron transfer steps involved in copper reduction. It was found that Fe^{2+} ions affect the electrodeposition kinetic by slowing down reaction kinetics, particularly the second electron transfer reaction.

Table of Contents

Chapter 1

Introduction

Part I: Motivation

Understanding the reduction kinetics of copper electrodeposition in a concentrated sulfuric acid electrolyte is of particular interest to the copper industry. At the extraction and purification stage, copper anode electrorefining and copper electrowinning are essential steps. In both cases, the metal deposited on the cathode needs to be periodically recovered, requiring the deposit to remain structurally stable throughout the duration of metal growth. In downstream copper applications, such as in electronics, the presence of voids or the lack of sufficient nuclei coalescence in electrodeposits can ultimately compromise the integrity of the product, e.g. computer chips. This last issue has recently been driving work to improve deposit quality[1–3], but less work has been published on the challenges faced in upstream copper production.

Factors influencing copper electrodeposits have been reported in conditions simulating the low pH, high concentration electrolytes common in industrial conditions.[4–6] In copper electrodeposition for extraction processes, solution additives play an important, though only marginally understood, role in the final deposit quality. Additives encompass both inevitable impurities inherited from the raw minerals and carried along with copper during the smelting process[7], as well as molecules purposely added to improve the deposit properties[8]. The outcome on deposit quality varies widely[6–10], with additives exhibiting either a positive or negative effect on the growing copper. Of particular interest in this work, Fe^{2+} ions have been reported to have a positive effect[3,6], possibly due to slowing down the

reduction kinetics of Cu^{2+}.[9] Because upstream copper production involves deposition on copper cathodes, we limit our study to copper deposition on a copper electrode. Thus, our study is not one of copper nucleation during electrodeposition, but rather speaks about electrodeposition kinetics during growth.

Part II: Brief Review of Literature

The electrodeposition of copper has been reported to occur through a two-step electron transfer mechanism, with the first electron transfer being the rate-limiting step[11,12]. Subsequent researchers have built upon this mechanism[13,14], taking into account intermediate chemical reaction steps related to the deaquation of solvation shells[15–17], as well as investigating the potential at which copper ion adsorption occurs[18]. Certain aspects of copper reduction kinetics remain highly contested, especially when comparing various electrolyte media and pH ranges,[19] partially due to difficulty in discerning the second electron transfer reaction.

Very few studies report the use of alternating current methods, including alternating current voltammetry (ACV) for copper electrodeposition[14]. The advantages of ACV methods were put forward by Smith[20], and more recent works by Bond has popularized the technique.[21] ACV offers the experimentalist the ability to separate faradaic components of the current response from nonfaradaic components, and to ultimately extract more accurate kinetic parameters[22,23]. This ability to filter out components of the current response, such as the double layer capacitance, allows for electrode phenomena not easily seen in DC voltammetry

methods to be investigated[24]. Some predictions have been made as to the expected AC current response for an adsorbed species[25], although to the authors' knowledge, there have not been many theoretical or experimental studies to determine what such a current response would look like during electrodeposition.

The practical objective of this work is to characterize the multiple steps involved in copper electrodeposition, with particular attention to the effect of Fe^{2+} on deposition kinetics. Technically, and in order to understand the cause of the possible kinetics effects, ACV is used to establish the electrochemical mechanism of copper electrodeposition.

Chapter 2

Theoretical Background

Part I: Copper Electroreduction Kinetics

Electrodeposition is a complex process drawing on metaphysics, not only chemistry but also solid-state physics, electronics, materials science [26]. A two electron reduction process for the deposition of a metal such as copper given by:

$$M^{2+} + 2e \rightarrow M \tag{2.1}$$

actually involves many interrelated kinetic processes, such as mass transport, charge transfer, followed by adatom diffusion, eventual incorporation into growth sites, and crystallization, each governed by their own rates.[27] The situation is further complicated in practical applications, e.g. copper electrodeposition, where a four-step mechanism, commonly referred to as an (C)ECE reaction, is involved[16].

$$Chemical\ reaction\ (C) \qquad Cu^{2+}(H_2O)_6 \overset{-xH_2O}{\Longleftrightarrow} Cu^{2+}(H_2O)_{6-x} \tag{2.2}$$

$$Electron\ transfer\ (E) \qquad Cu^{2+}(H_2O)_{6-x} \overset{e^-}{\Leftrightarrow} Cu^{+}(H_2O)_{6-x} \tag{2.3}$$

$$Chemical\ reaction\ (C) \qquad Cu^{+}(H_2O)_{6-x} \overset{-yH_20}{\Longleftrightarrow} Cu^{+}(H_2O)_{6-x-y} \tag{2.4}$$

$$Electron\ transfer\ (E) \qquad Cu^{+}(H_2O)_{6-x-y} \overset{e^-}{\Leftrightarrow} Cu(O) \tag{2.5}$$

Such a mechanism involves a chemical reaction (C), in this case the dehydration of the hydration shell surrounding Cu^{2+}; an electron transfer (E), the reduction of Cu^{2+} to Cu^{+}; a second chemical reaction (C), the hydrolysis or dehydration of Cu^{+}; and a second electron transfer step (E), the reduction of Cu^{+} to Cu metal.

Of the two electron transfer steps involved in copper reduction, the first (Equation 2.2) is reported as rate-limiting[12]. Under certain conditions, such as electrolytes approaching a neutral pH, copper reduction exhibits clearly only one electron transfer[19]. For the purposes of this study, the kinetics of these two reduction reactions will be the main focus, in order to better understand the charge transfer mechanisms and determine how the electrolytic conditions affect them.

The current density, i, can be related to the overpotential η, the potential difference between a theoretical Nernstian potential and the experimentally observed potential of reaction , through the Butler-Volmer equation[28,29]

$$i = i_o \left[\exp\left(\frac{\alpha z F \eta}{RT} - \frac{(1-\alpha) z F \eta}{RT}\right) \right] \tag{2.6}$$

where α is the transfer coefficient, F is the Faraday constant, R is the molar gas constant, z is the ion charge magnitude, i_0 is the exchange current density, and T is the system temperature. While this equation holds true strictly for one-electron, one-step processes, it has been used as an approximation for two-step electron transfer processes. Furthermore, with a sufficiently high overpotential, the anodic contribution becomes very small and one may consider a limiting equation as

$$i = i_o \left[\exp\left(\frac{\alpha z F \eta}{RT}\right) \right] \tag{2.7}$$

with i_0 and α being kinetic parameters of the reaction determined through experimentation or modeling.[30]

Part II: Alternating Current Voltammetry

Copper electrodeposition involves multiple processes that complicate the current response. Some of these processes can be separated into faradaic components, e.g., charge transfer, and non-faradaic components, e.g., double layer capacitance. For this reason, alternating current cyclic voltammetry (ACV) offers an experimental advantage. Because faradaic processes respond to voltage in a nonlinear fashion, and non-faradaic processes respond linearly, it is possible to separate the two processes using ACV[21]. The linear terms, i.e. the non-faradaic processes caused by double layer capacitance effects, will only be present in the DC current response and the first fundamental harmonic AC response[21,23]. Being able to isolate faradaic processes in voltammetry is advantageous to this study, as it will allow examination of charge transfer kinetics without interference from non-faradaic components. In addition, ACV techniques are useful in examining very fast kinetic reactions[21]. This is ideal for studying copper deposition kinetics because Cu^+ reduction (Equation 2.5) is a very fast step.

In ACV experiments, an AC waveform, such as a sine wave, is superimposed onto a linear DC potential sweep. The current response can then be converted into the frequency domain via a Fast Fourier Transform. In a plot of power versus frequency, the DC component of the current response is given by a sharp peak near zero frequency. Additional peaks, occurring at multiples of the AC wave's frequency,

called the harmonics, represent the AC components of the current response[20]. These individual peaks can be isolated and converted back into the time domain to separately look at the current contribution of each harmonic[21]. This separates the AC responses from the DC response, the faradaic components from the non-faradaic components (Figure 2.1)

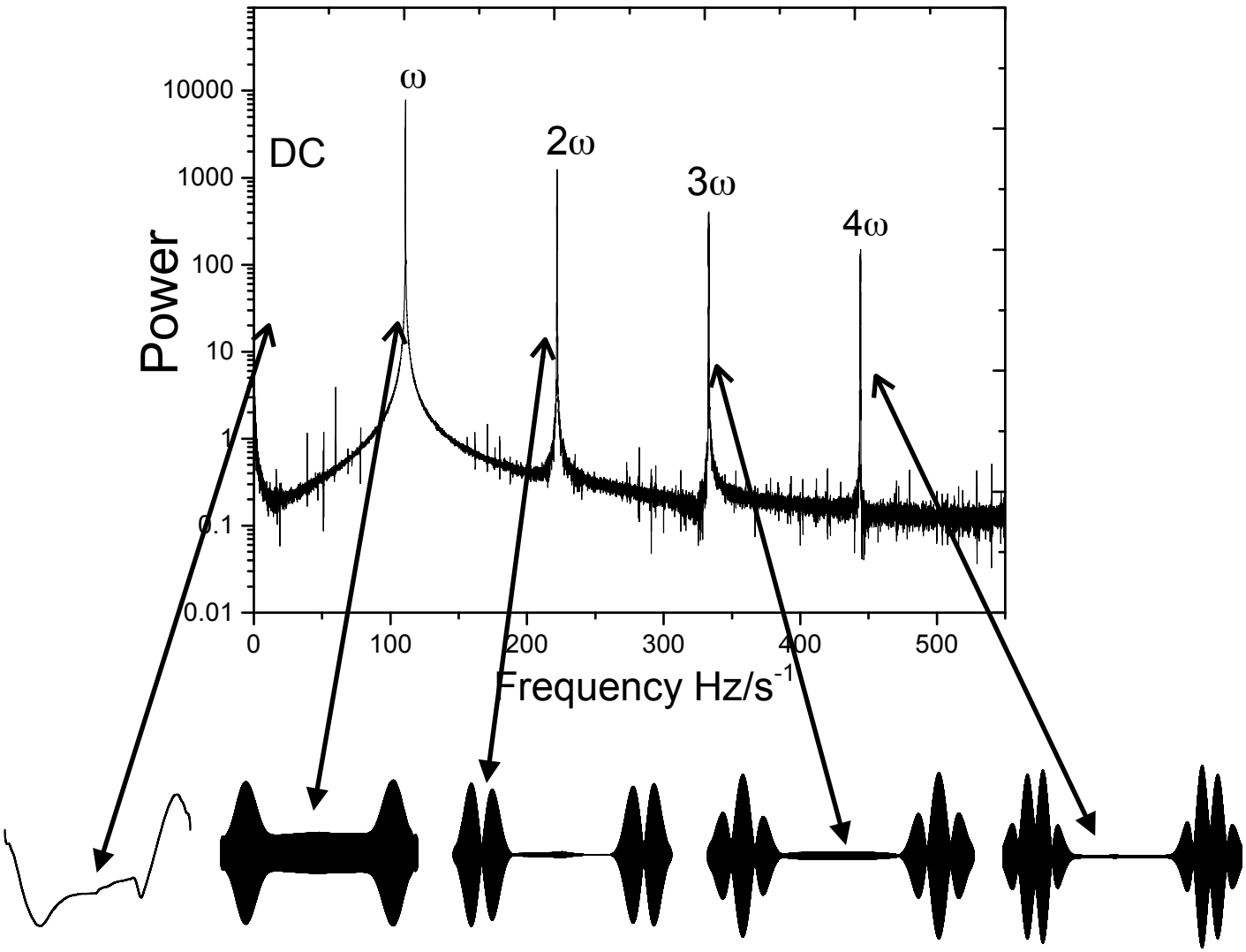

Figure 2.1: Fourier transform of AC current response (frequency domain) with selected AC current responses from higher harmonics (time domain)

Chapter 3

Procedures and Experimental Methods

Part I: Experimental Setup

A double-walled glass container was used as the electrochemical cell hosting a three electrode setup (Figure 3.1). The working electrode was a 6.58 mm diameter rotating copper disk**.** The counter electrode was a coiled platinum wire, and the reference electrode was a saturated calomel electrode (0.241 V vs. SHE at RT). All potentials are hereafter reported with respect to the standard hydrogen electrode. Solutions were prepared using reagent-grade sulfuric acid (95-98% purity, Sigma-Aldrich), copper (II) sulfate pentahydrate (99% purity, Alfa Aesar), and iron (II) sulfate pentahydrate (99+% purity, Alfa Aesar), and deionized water. Powders were weighed first, to obtain the necessary amount of cupric and ferrous ion concentration, and then dissolved over a twenty-four hour period into a solution with the desired molarity of sulfuric acid.

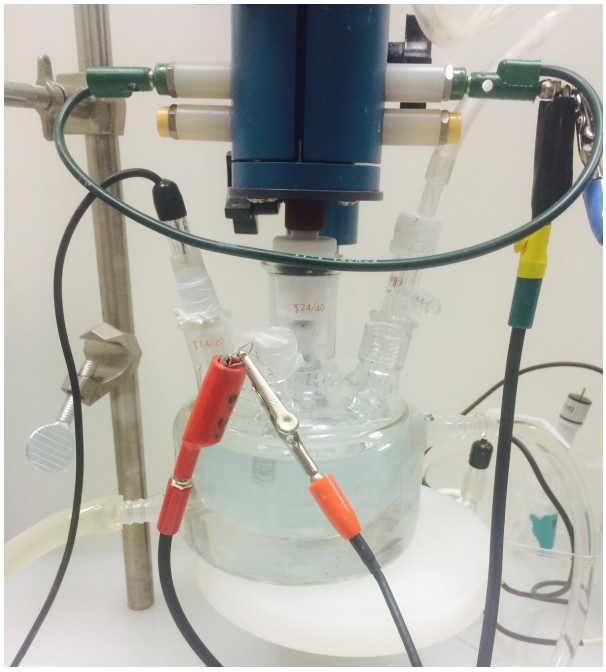

Figure 3.1: Experimental electrochemical cell with three electrode configuration

Experiments were either performed at ambient temperature 298 ± 5 K or at water's freezing point, 273 K. For the later, temperature was controlled by flowing ice water through the cell wall. The working electrode was polished to a mirror with 1 micron alumina and nitrogen gas was bubbled through all electrolytes for at least 10 minutes prior to experimentation. The copper disk was rotated at 800 rpm throughout all rotating disk measurements. A summary of experimental solutions and conditions may be found in Table 3.1

Each solution was first characterized using electrochemical impedance spectroscopy to determine the uncompensated resistance obtained at the limit Z_{im} approaches 0 at 100 kHz on a Nyquist plot. The measured resistance was used to correct for the IR drop in post-experiment analysis, following:

$$Ereal = Emeas - Imeas*R \quad (3.1)$$

All data are presented with respect to this corrected potential.

Table 3.1: Experimental conditions of prepared solutions

	Solution 1a	Solution 1b	Solution 1c	Solution 2a	Solution 2b	Solution 2c	Solution 3	Solution 4
H_2SO_4 (M)	**1.84**	**1.08**	**.89**	**1.84**	**1.08**	**0.89**	**1.84**	**1.84**
Expected E^0 H^{2+}/H_2 (V/SHE)	**0.008**	**.001**	**0**	**0.008**	**.001**	**0**	**.007**	
Cu^{2+} (M)	**0.63**	**0.63**	**0.63**	**0.63**	**0.63**	**0.63**	**0.01**	**0.01**
Expected E^0 Cu^{2+}/Cu (V/SHE)		**0.334**			**0.334**		**0.286**	
Fe^{2+} (M)	-	-	-	**0.054**	**0.054**	**0.054**	-	**0.054**
Expected E^0 Fe^{2+}/Fe (V/SHE)	-	-	-		**-0.515**		-	**-0.509**
Temperature (K)			**298**				**273**	
AC amplitude (mV)			**160**				**80**	
AC frequency (Hz)					**7.75**			

Measurements were conducted for no more than 5 cycles with each freshly polished electrode when the working electrode was rotating. The investigated potential range was chosen to limit the hydrogen evolution reaction, to limit anodic dissolution of the copper electrode, and to ensure repeatability between cycles in both the DC component and higher AC harmonics. Only the third, fourth, and fifth cycles were analyzed. Non-rotating experiments were only run for one cycle. At the end of the last cycle, the cell was dismantled and the electrode was re-polished before the next run.

Part II: Methods of Data Collection and Analysis

The direct current voltammograms were generated using a potentiostat (Reference 3000: Gamry Instruments, USA). For alternating current measurements, a sine wave created with a waveform generator (MOTU UltraLite-mk3 Hybrid: MOTU, USA) was superimposed onto the direct current ramp. The current response was collected using a data acquisition system (DT9837B: Data Translation, USA) at 25000 Hz acquisition frequency. A custom designed code (ver. 5.5.2; Scilab Enterprises, France) was used to analyze the results post-measurement. The complex current response was analyzed using a Fast-Fourier Transform (FFT), which presented a power spectrum with sharp peaks at multiples of the frequency of the AC sine wave. These peaks represented the transformed DC, fundamental, and higher harmonic components, and were isolated and converted back into the time domain using an

inverse FFT. Thus, the DC and harmonic results could be individually plotted versus the DC potential[21].

In absence of a full model for a (C)ECE mechanism involving adsorption, the resulting components were compared to a model drawn from experimental results for a more simplified case: a reversible, single electron transfer system involving the ferri/ferrocyanide redox couple with 10 mM $Fe(CN)_6^{3+}$ and 3M KCl (Figure 3.2). Under these conditions, the fundamental harmonic presents one sharp, symmetrical peak at the half wave potential, $E_{1/2.}$ The second harmonic is represented by the derivative of the fundamental harmonic, with two symmetrical peaks and a trough at $E_{1/2}$. The third harmonic is a derivative of this second harmonic, with three peaks, the middle of which is located at $E_{1/2}$. This pattern repeats for all higher harmonics[20]. In this system, peak heights scale proportionally with an increase in the electron transfer coefficient, α, and with faster rate constant k_0. A large α favors more symmetrical peaks, in both height and shape[22]. Four main features were then of interest in analyzing experimental results: peak heights on both the anodic and cathodic sides of $E_{1/2}$, peak shape symmetry with respect to $E_{1/2}$, overall peak height, and the location of $E_{1/2.}$

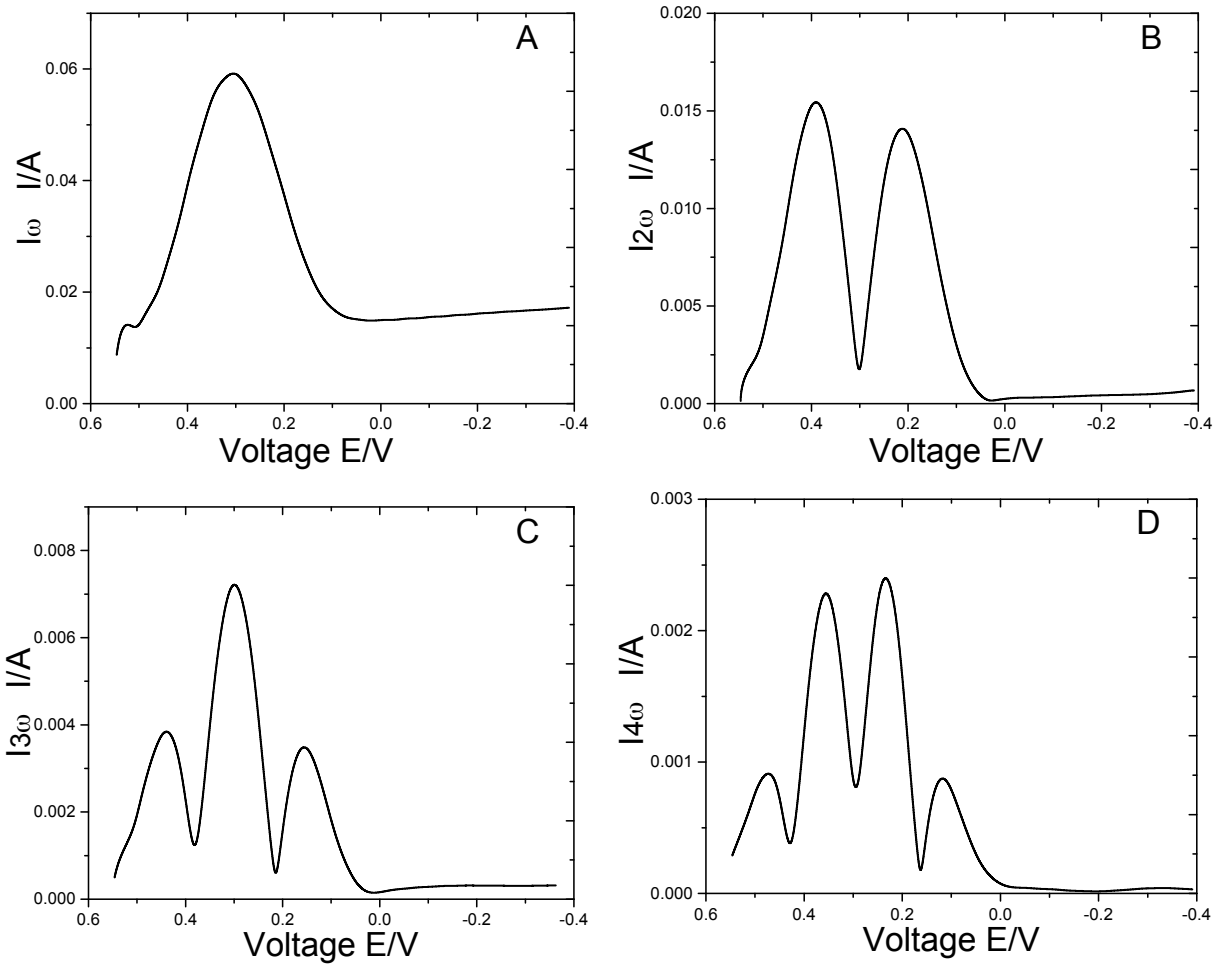

Figure 3.2: Extracted AC harmonic components A) fundamental B) second C) third D) fourth harmonic component for Ferri/Ferrocyanide redox couple.

Chapter 4

Results

Part I: Electrodeposition in Industrial Conditions

Figure 4.1 shows the DC signal measured during copper electrodeposition in a solution with 0.063 M Cu^{2+} and 1.85 M H_2SO_4, conditions representative of industrial practices. Multiple analyses of the DC component does not allow one to clearly distinguish the current responses for solutions with and without 0.054 M Fe^{2+}.

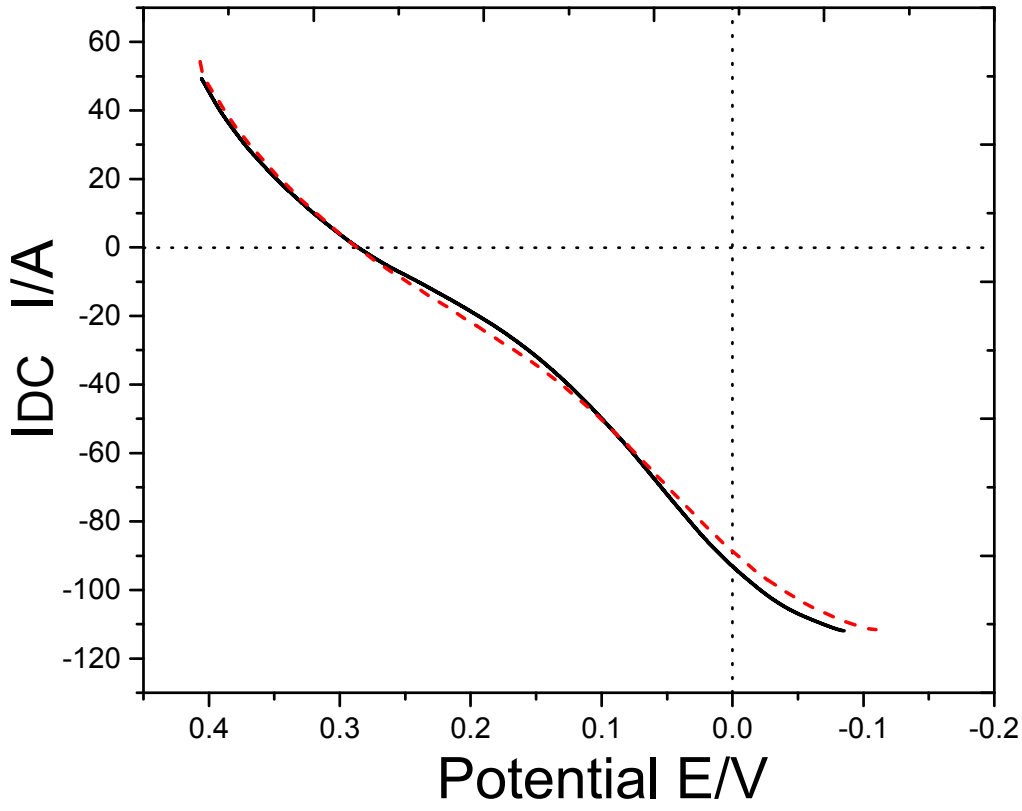

Figure 4.1: DC Current response for 1.84 [M] H_2SO_4, 0.64 [M] Cu^{2+} black, solid: 0 [M] Fe^{2+} red, dotted: 0.054 [M] Fe^{2+} at ambient temperatures

On the other hand, as shown in Figure 4.2, analysis of the fundamental and higher harmonic components in a solution with 0.630 M Cu^{2+} with 1.84, 1.08, or 0.89 M H_2SO_4 revealed harmonic peaks characteristic of a faradaic event. The peak center for this faradaic event shall henceforth be denoted E_1. The locations of each harmonic peak potential in various concentrations of H_2SO_4 are summarized in Table 4.1. $E_1^{fundamental}$, as observed from the fundamental harmonic, does not align with the E_1 as observed in higher harmonics.

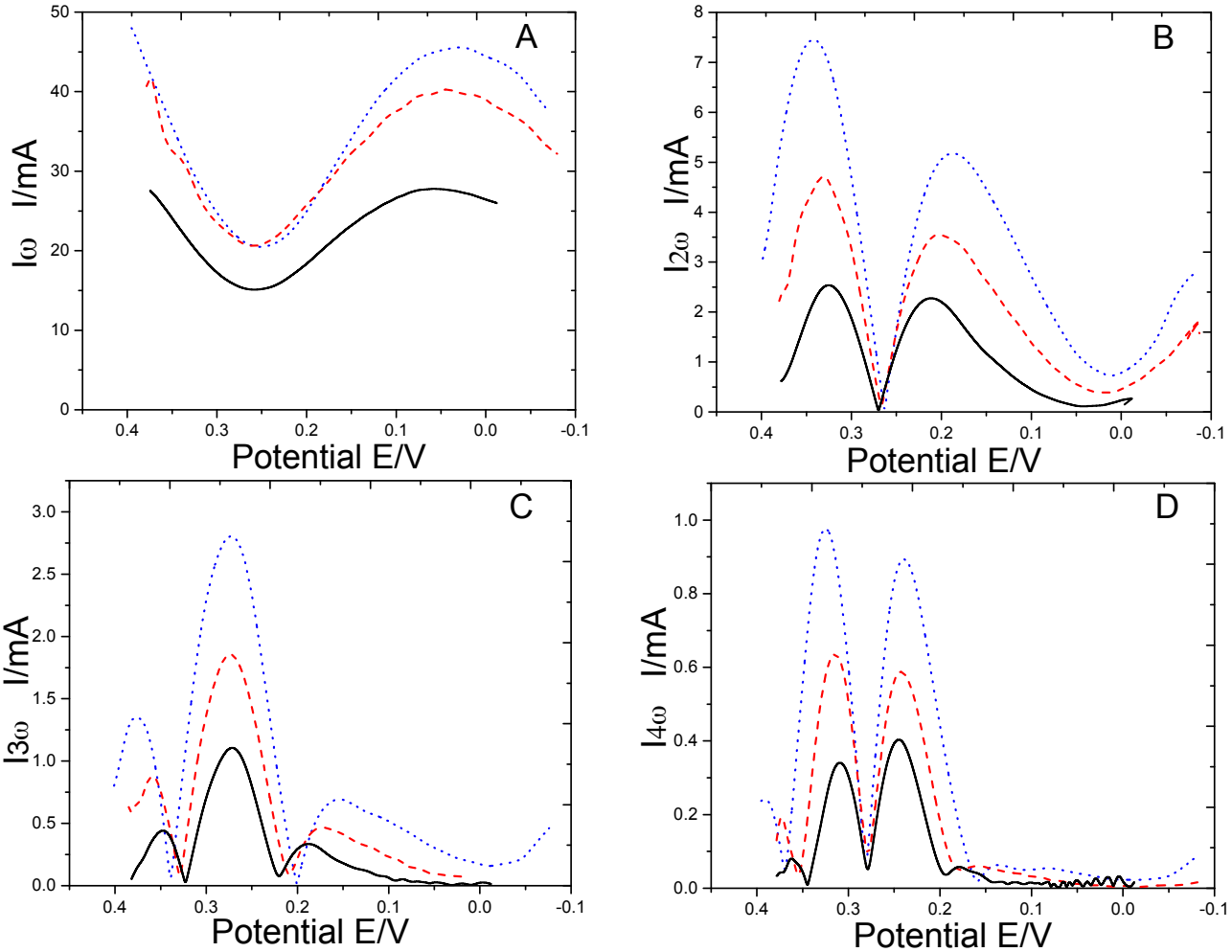

Figure 4.2: Harmonic current response for experiments simulating industrial conditions without Fe^{2+} A) fundamental harmonic B) second harmonic C) third harmonic D) fourth harmonic. Black, solid: 0.89 [M] H_2SO_4 Red, dashed: 1.08 [M] H_2SO_4 Blue, dotted 1.84 [M] H_2SO_4

Table 4.1: Locations of current response peaks in fundamental and higher harmonics for various concentrations of H_2SO_4, no Fe^{2+} present in system

	$E_1^{Fundamental}$	E_1^{Second}	E_1^{Third}	E_1^{Fourth}
1.84 [M] H_2SO_4	0.03 V /SHE	0.27 V /SHE	0.27 V /SHE	0.28 V /SHE
1.08 [M] H_2SO_4	0.04 V /SHE	0.27 V /SHE	0.27 V /SHE	0.28 V /SHE
0.89 [M] H_2SO_4	0.06 V /SHE	0.27 V /SHE	0.27 V /SHE	0.28 V /SHE

At higher concentrations of H^+, the peaks become asymmetric with respect to E_1. In a solution with 1.84 M H_2SO_4, there is a considerable peak height difference between the two peaks of the second harmonic. In the third and fourth harmonic, the peaks that occur on the anodic side of E_1 are higher than their cathodic counterparts. This difference in peak height becomes less noticeable as the concentration of H^+ increases. In the extreme case of 0.84 M H_2SO_4, this situation is reversed in the fourth harmonic; the peaks on the anodic side of E_1 are lower than their cathodic counterparts.

The peak shapes are also asymmetrical with respect to E_1. In solutions with higher concentrations of H^+, the peaks at potentials cathodic to E_1 have a prominent shoulder around 0.15V /SHE, which is absent from their anodic counterparts. This shoulder is less distinguishable in solutions with a higher pH.

Figure 4.3 shows the second and third harmonics for solutions that contained 0.054 M Fe^{2+} ions. All of the key features of the AC harmonics discussed above for solutions without Fe^{2+} (Figure 4.2) were more pronounced in solutions containing

Fe^{2+}. This is illustrated by the prominence of the shoulder at 0.15 V /SHE in such solutions. Likewise, the peak heights are more asymmetric than their ironless counterparts. In solutions with 0.84 M H_2SO_4, the peak heights on the anodic side of E_1 remain higher than their cathodic counterparts, even in the fourth harmonic. In solutions with high concentrations of H^+, peak heights were lower when Fe^{2+} ions were present. Such solutions also show wider harmonics peaks, with the anodic and

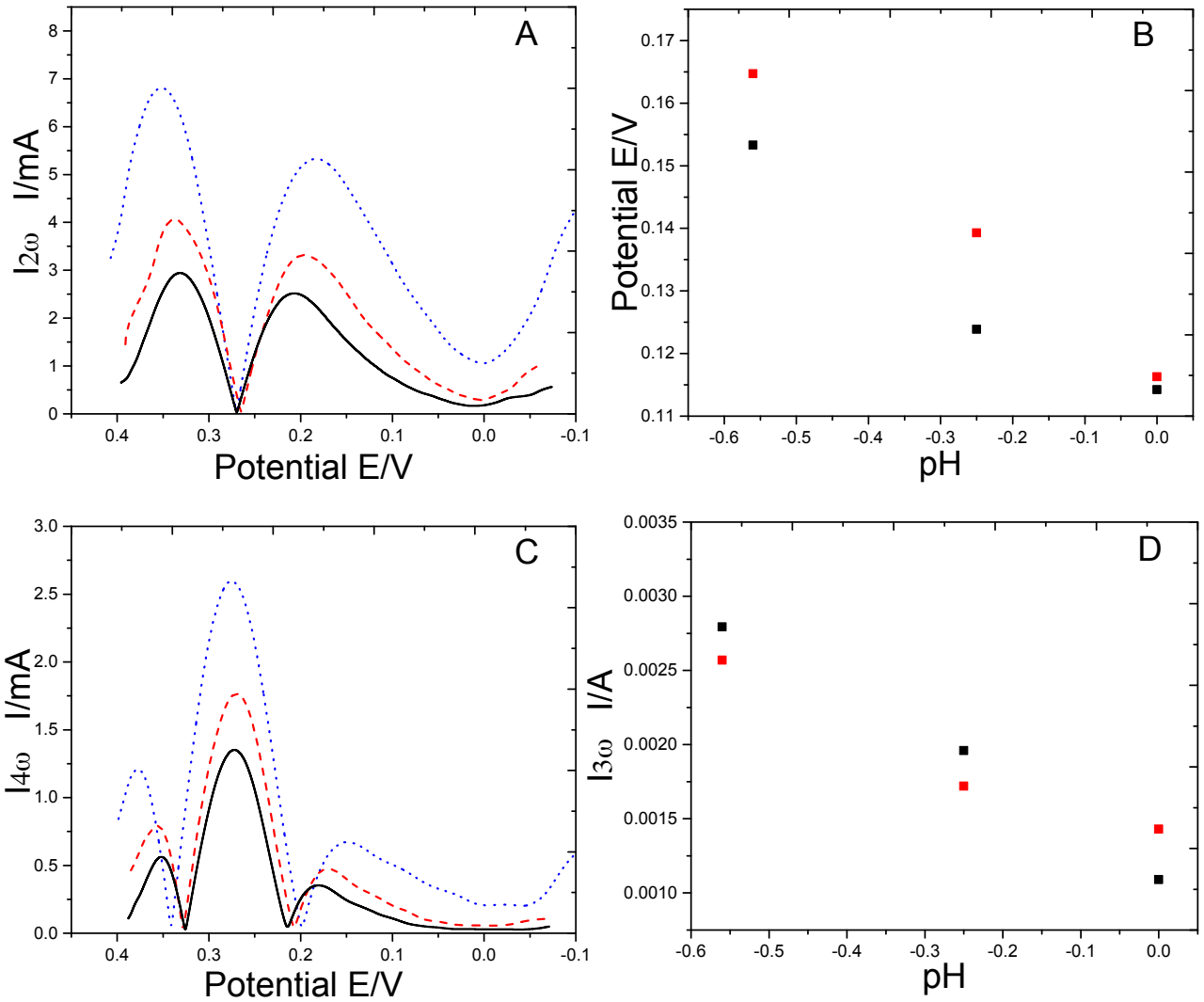

Figure 4.3: A) Second harmonic current response for experiments simulating industrial conditions with Fe^{2+} B) Distance between second harmonic peaks with respect to pH. C) Third harmonic current response for experiments simulating industrial conditions with Fe^{2+} D) Location of third harmonic with respect to pH. Harmonic plots: Black, solid: 0.89 [M] H_2SO_4 Red, dashed: 1.08 [M] H_2SO_4 Blue, dotted 1.84 [M] H_2SO_4 pH plots: Black: no Fe^{2+} Red: Fe^{2+} present [M] H_2SO_4

cathodic sides located further from each other. As with peak height, this effect is less pronounced at a higher pH.

Part II: Electrodeposition in Slow-Kinetic Conditions

In order to investigate the possibility that the peak shoulder located at 0.15 V /SHE was a second faradaic event, efforts were made to slow down electron transfer kinetics. The next set of experiments diverged from industrial conditions in favor of colder temperatures (273 K) and lower concentrations of Cu^{2+}. The next set of solutions were prepared with 0.01 M Cu^{2+} and 1.84 M H_2SO_4, both with and without 0.054 M Fe^{2+}. Cyclic voltammetry experiments under these conditions (Figure 4.4) still do not show a significant difference between solutions with and

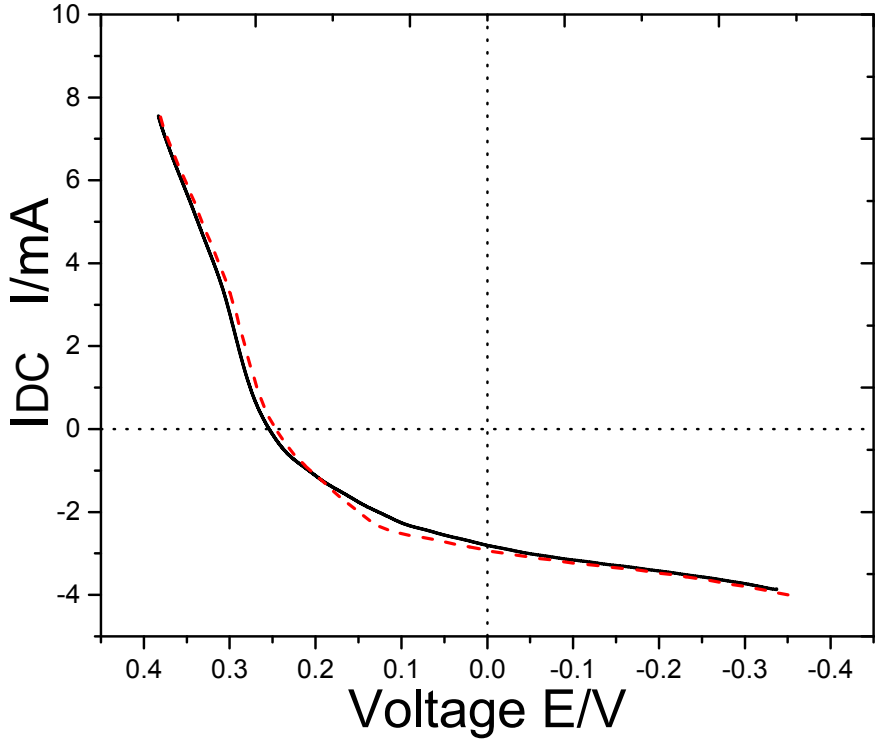

Figure 4.4: DC Current response for 1.84 [M] H_2SO_4, 0.01 [M] Cu^{2+} black, solid: 0 [M] Fe^{2+} red, dotted: 0.054 [M] Fe^{2+} at 273 K

without Fe^{2+}. Figure 4.5 compares the fundamental and second harmonic (overlaid) from a room temperature measurement containing 0.63 M Cu^{2+}, 1.84 M H_2SO_4, and 0.054 M Fe^{2+}, with the fundamental and second harmonic (overlaid) from a freezing point measurement containing 0.01 M Cu^{2+}, 1.84 M H_2SO_4, and 0.054 M Fe^{2+}.

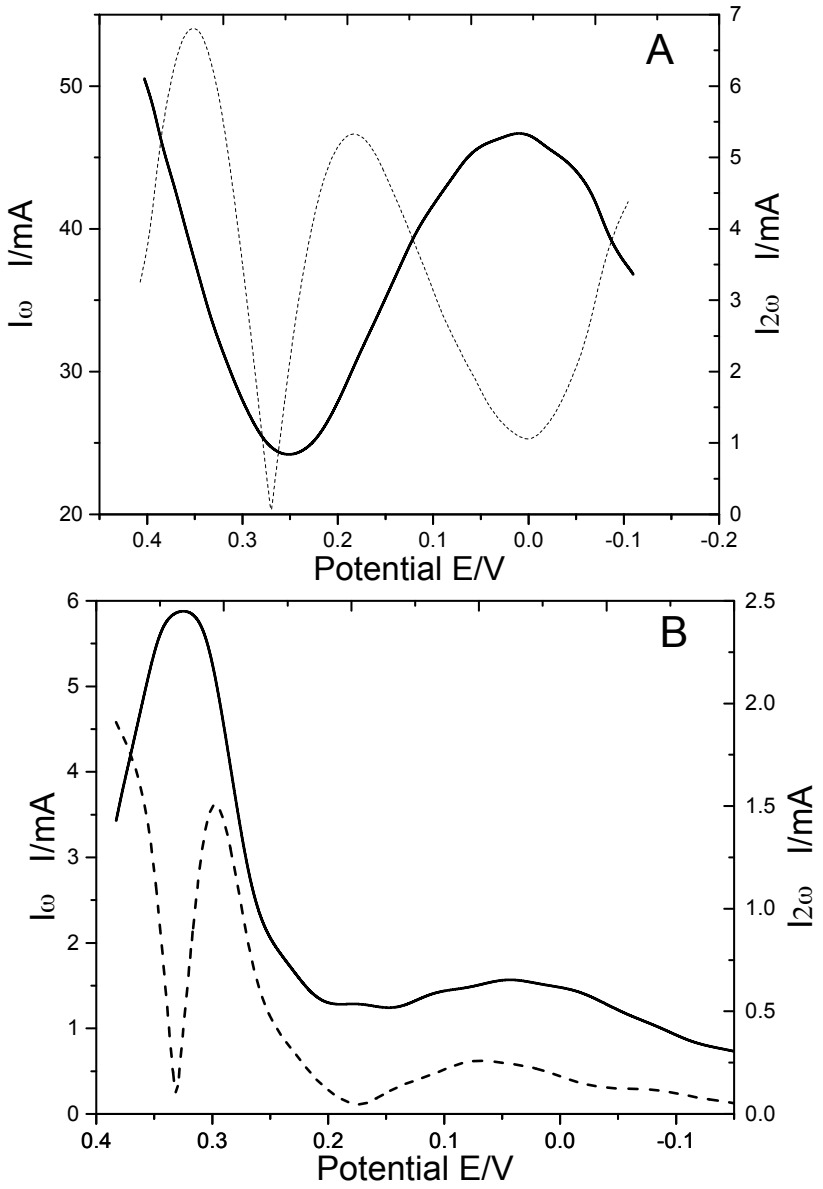

Figure 4.5: A) Overlaid fundamental (solid) and second (dashed) harmonic current response for 1.84 [M] H_2SO_4, .63 [M] Cu^{2+} .054 [M] Fe^{2+} at 298 K B) Overlaid fundamental (solid) and second (dashed) harmonic current response for 1.84 [M] H_2SO_4, .01 [M] Cu^{2+} .054 [M] Fe^{2+} at 273 K

As anticipated for such conditions, reaction rates were slower. Two separate faradaic events can be observed, at 0.33 V/SHE and 0.04 V/SHE, termed E_1 and E_2, respectively. Figure 4.5b shows these two distinct fundamental harmonic peaks, which line up with two distinct second harmonic troughs. The location of E_1 in Figure 4.5b is shifted anodically with respect to Figure 4.5a.

Figures 4.6 and 4.7 show the harmonics for the isolated first and second faradaic events, respectively. As observed at room temperature, harmonic peaks in solutions with Fe^{2+} were wider than solutions without Fe^{2+}. Figure 4.6 shows no significant difference in peak height or shape in solutions without or without Fe^{2+}. The current response at E_2 (Figure 4.7) shows consistently lower harmonic peaks with enhanced separation between the cathodic and anodic sides of E_2. Compared to the harmonics at E_1, and the results of the model, the E_2 peaks are atypical. E_2^{third} and E_2^{fourth} are located at a more cathodic potential than $E_2^{fundamental}$ or E_2^{second}. This shift is similar to the one observed in Figure 4.2. The observed faradaic event at E_2 is distorted towards the more anodic potential due to overlap with the faradaic event at E_1, with the strongest effect on the fundamental harmonic. Higher harmonics appear less susceptible to such overlap, pertaining more strictly to the charge transfer of interest, with peak positions stabilizing in the third and fourth harmonic.

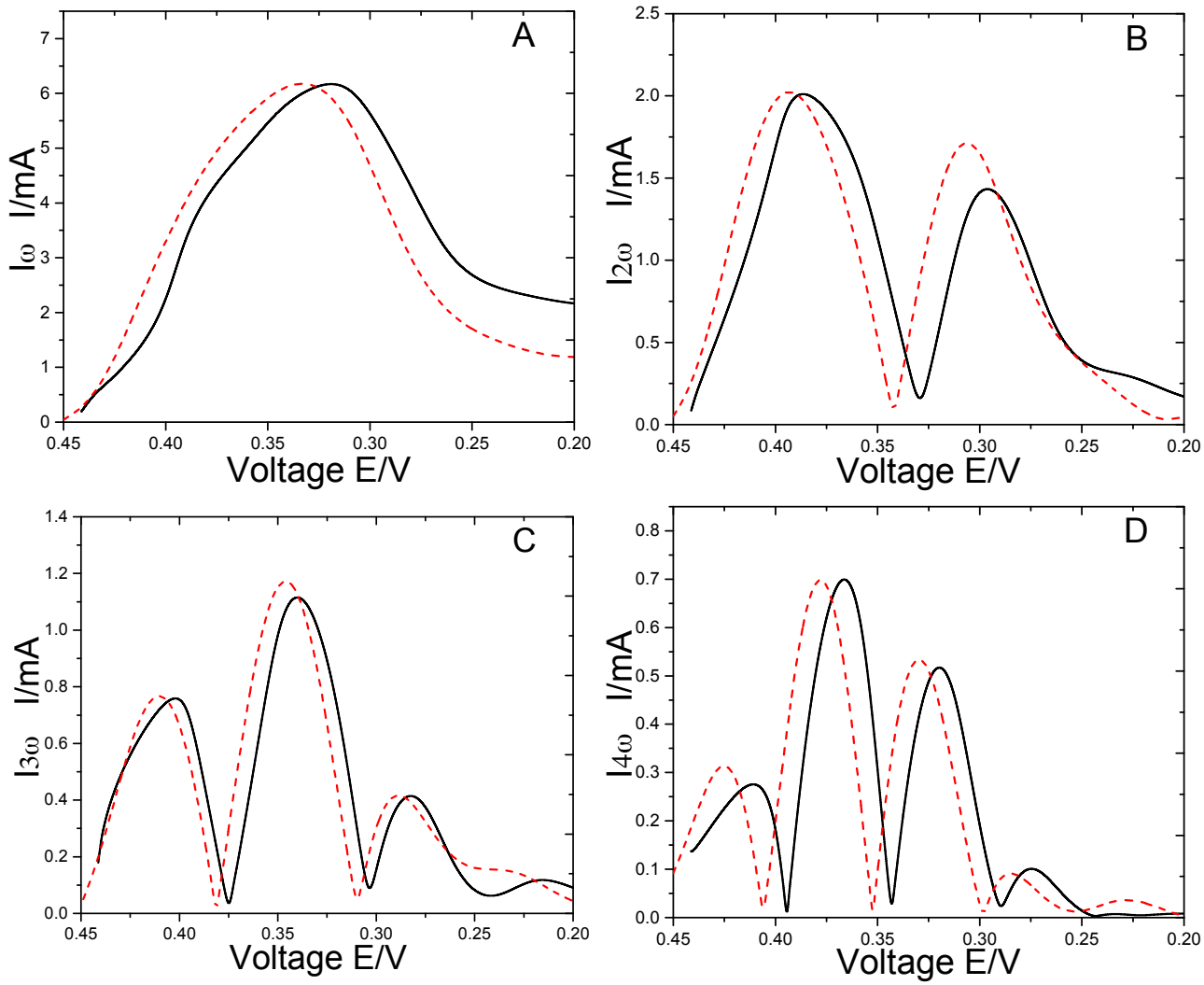

Figure 4.6: Harmonic current response at E_1 for experiments at 273 K, 1.84 [M] H_2SO_4, 0.01 [M] Cu^{2+} A) fundamental harmonic B) second harmonic C) third harmonic D) fourth harmonic. Black, solid: no Fe^{2+} Red, dashed: 0.054 [M] Fe^{2+}

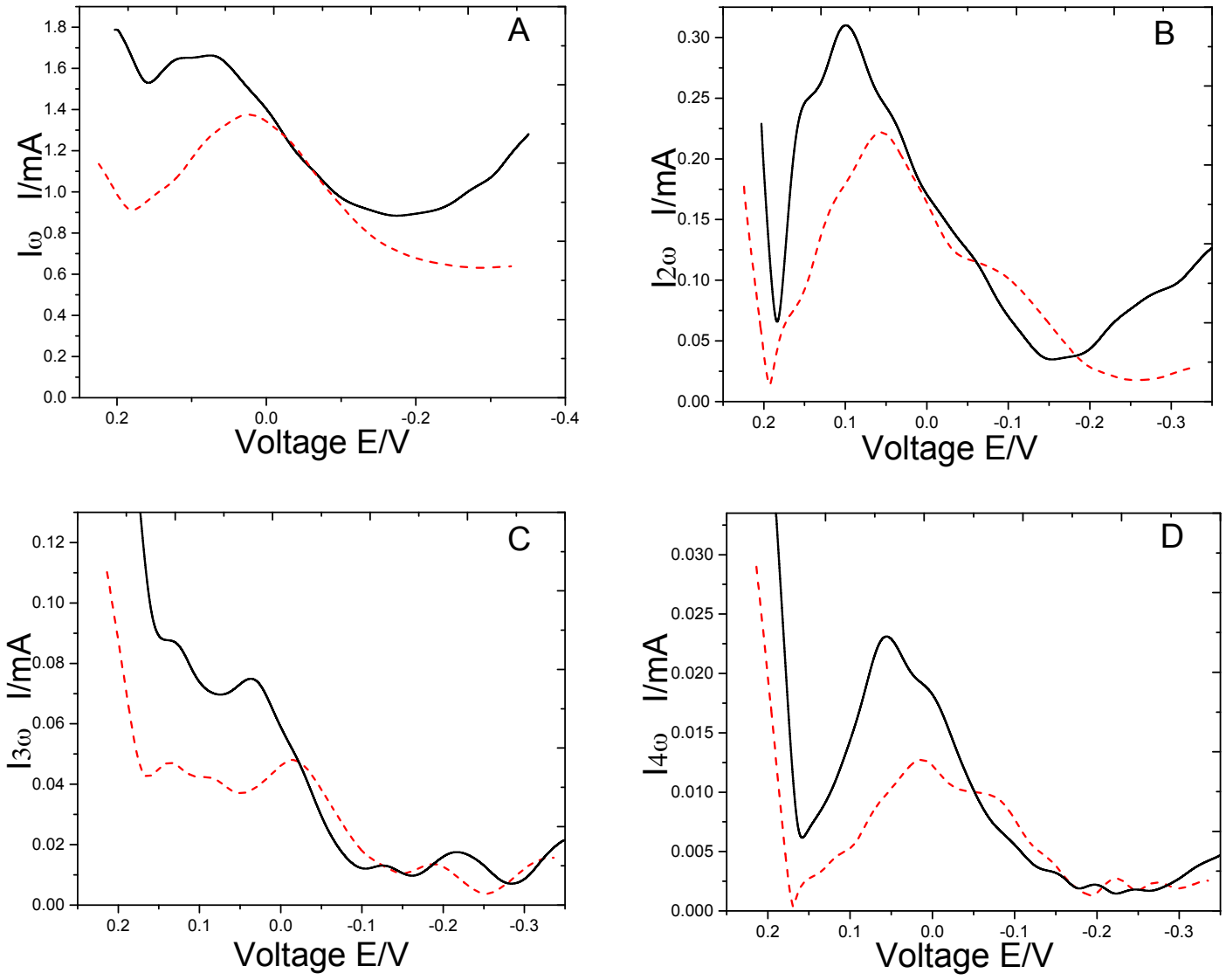

Figure 4.7: Harmonic current response at E_2 for experiments at 273 K, 1.84 [M] H2SO4, 0.01 [M] Cu^{2+} A) fundamental harmonic B) second harmonic C) third harmonic D) fourth harmonic. Black, solid: no Fe^{2+} Red, dashed: 0.054 [M] Fe^{2+}

Although the peaks at E_2 are strongly asymmetrical, they split at a consistent potential with alternating peaks (for odd harmonics) and troughs (for even harmonics). This is a definitive characteristic for a faradaic event in AC voltammetry, with the observed asymmetry being typical of an irreversible reaction[20,25]. Such a current response shape has also been predicted for reactions involving an adsorption step[25].

In order to further investigate the electron transfers occurring at E_1 and E_2, measurements were taken keeping the working electrode stationary (Figure 4.8). The absence of rotation did not affect E_1 signals, while peak currents at E_2 increased. Furthermore, the harmonics at E_2 exhibit a closer shape to E_1, in qualitative agreement with the model.

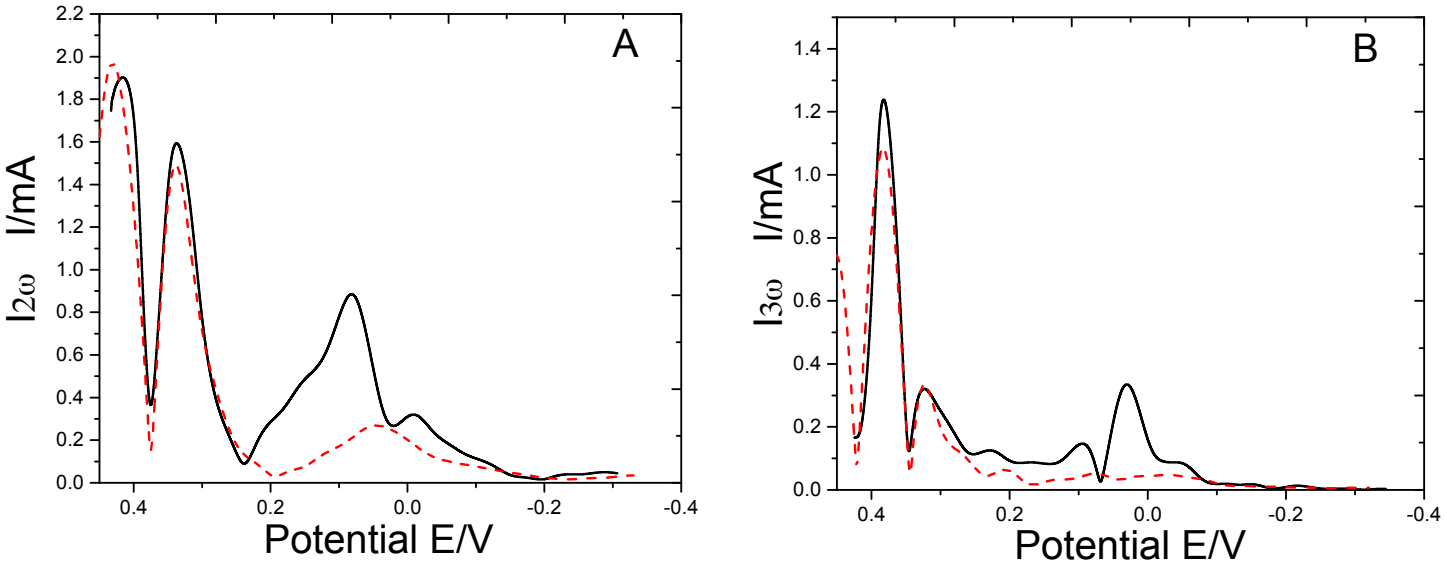

Figure 4.8: Harmonic current response for experiments at 273 K, 1.84 [M] H2SO4, 0.01 [M] Cu^{2+}, 0.054 [M] Fe^{2+} A) second harmonic B) third harmonic
Black, solid: no rotation Red, dashed: W.E. rotated at 800 RPM

Chapter 5

Discussion

Part I: The Mechanism of Copper Electroreduction

Depending on the experimental conditions highlighted earlier, one or two faradaic events may be distinguished during copper electrodeposition. In industry-simulating conditions, at higher temperature and in the presence of high concentrations of copper, DC measurements indicate an inflection point at 0.25 V/ SHE, a distinct event E_1 which is also observed at a similar potential in AC measurements in second and higher harmonics. At lower temperatures, the location of E_1 shifts anodically, as would be expected from a system with Nernstian behavior. The location of E_1 at a potential close to the standard electrode potential for Cu^{2+} reduction to Cu metal (Table 4.1), and the lack of any other possible faradaic reactions occurring at that potential allows us to assign E_1 to the following reaction:

$$reaction\ 1 \qquad Cu^{2+} \overset{e^-}{\Leftrightarrow} Cu^{+} \qquad \text{(slow)} \qquad 5.1$$

DC measurements in industrial conditions also indicate a second inflection point at 0.05 V /SHE, E_2, an event not noticed as easily as E_1 in AC measurements under the same conditions. Instead, the second and third harmonic currents from E_1 exhibit shoulders overlapping with the current response at E_2. The shoulders are most prominent in low pH solutions, which have been shown to be associated with a smaller α[16,31]. The decrease in symmetry could be attributed to a decrease in α, or to the increasing prominence of the event E_2. Slowing overall reaction kinetics, either through decreasing pH, decreasing Cu^{2+} concentration, or decreasing temperature,

points to slower events at E_1 and E_2, increasing the prominence of this shoulder. Furthermore, at low pH, the harmonics at event E_1 are more asymmetrical, again indicating current overlap from E_2. This overlap is consistent with ACV models for multiple electron transfer steps[20].

In the extreme case shown in Figures 4.6, 4.7 and 4.8, the two reduction steps at E_1 and E_2 are completely separated. In these cold solutions with low concentrations of Cu^{2+}, no shoulders on the cathodic side of the reaction are observed. This confirms that the second event corresponds to a distinct electron transfer reaction, and that the shoulders observed under industrial conditions are due to the overlap of E_1 and E_2 currents. It is likely, therefore, that the event E_2 is very fast compared to E_1, such that it is often masked by E_1 current responses. The event E_2 exhibits atypical higher harmonic (> 2ω) currents with low currents having strongly asymmetrical shapes, pointing to an irreversible reaction or a reaction involving an adsorbed species[20,25].

It is possible that the hydrogen evolution reaction (HER) occurs in parallel with the reaction at E_2, although studies of hydrogen evolution on copper electrodes report large overpotentials for the HER [4,5,32]. Furthermore, Fe^{2+} has been shown to be a catalyst for HER[32], which contradicts the decrease in currents observed for E_2 in systems in the presence of Fe^{2+} (Figure 4.7).

Results with a stationary working electrode show E_2 has a stronger dependence on rotation than E_1, with the event E_2 appearing more distinct and better defined. In non-rotating conditions, mass transfer quickly controls the AC current for the dissolved species, and the enhanced separation between E_1 and E_2

suggests that E_1 involves bulk solution species, while E_2 mostly depends on surface species, e.g. adsorbed species.

The faradaic event E_2 therefore appears as a fast electron transfer step involving surface confined species, most likely following reaction 2:

$$reaction\ 2 \qquad Cu^{+} \overset{e^{-}}{\Leftrightarrow} Cu \qquad \text{(fast)} \qquad 5.2$$

Previous authors have reported such a reaction occurring at similar potentials, suggesting that the reaction involves Cu^{+} as an adsorbed species.[18]

The features of the fundamental harmonics for this system recorded in industrial conditions remain anomalous, in particular with regards to the shift of $E_1^{fundamental}$ from the Nernst reduction potential for reaction 1. Such a shift is not observed in conditions where reaction 2 can be isolated, suggesting that the measured reduction potential for reaction 1 in industrial conditions represents a value between the Nernst potentials for reactions 1 and 2. This is also consistent with ACV models for a mechanism involving two successive electron transfer steps[20].

Part II: The Effect of Ferrous Ions

In industrial conditions, the effect of Fe^{2+} on the electron transfer kinetics is more predominant at low pH. With Fe^{2+} present in the electrolyte, the harmonic peaks for reaction 1 remain asymmetrical, even at a higher pH, as opposed to measurements without Fe^{2+}. This suggests that reaction 2, which has harmonics

better resolved at lower pH, is influenced by Fe^{2+}, the presence of which enhances the separation between reaction 1 and 2.

Under conditions where the two reduction steps are distinguishable, no difference in harmonic shape for reaction 1 in solutions with and without iron can be observed (Figure 4.6). Conversely, reaction 2 is highly influenced by the presence of Fe^{2+} (Figure 4.7). Measurements on solutions containing Fe^{2+} reveal consistently lower currents and shapes that more qualitatively fit the ACV model than measurements without Fe^{2+}.

When Fe^{2+} is present in the system, reaction 1 appears at more anodic potentials, while reaction 2 occurs at more cathodic potentials. Fe^{2+} ions therefore appear to be hindering reaction 2, thus enhancing separation between the two electron transfers, while not influencing reaction 1. It may be proposed that electrostatic effects from Fe^{2+} are hindering adsorption, which would not affect reaction 1. This is useful for isolating and studying the two reactions independently and extracting kinetic parameters for Cu^{+} reduction.

Our results allow us to propose that the electron transfers in copper reduction obey the following mechanism:

$$\begin{aligned} step\ 1 \quad & Cu^{2+} \overset{e^-}{\Leftrightarrow} Cu^{+} \\ step\ 2 \quad & Cu^{+} \overset{e^-}{\Leftrightarrow} Cu^{+}_{ads} \\ step\ 3 \quad & Cu^{+}_{ads} \overset{e^-}{\Leftrightarrow} Cu^{0}_{ads} \end{aligned} \qquad 5.3$$

The inconsistent trends with pH for step 3, however, may indicate that Fe^{2+} affects the intermediate chemical reaction:

$$Cu^{+}(H_20)_{6-x} \overset{-yH_20}{\Longleftrightarrow} Cu^{+}(H_20)_{6-x-y} \qquad 5.4$$

via interaction between the solvation shell around Fe^{2+} and the solvation shell around Cu^{+}.

Lack of a fully developed model for ACV experiments on a (C)ECE mechanism involving adsorption limits the extent to which kinetics for Cu^{+} reduction and the influence of Fe^{2+} on this reduction can be quantitatively characterized. It is proposed that future work be focused on developing such a model.

Chapter 6

Conclusions

The overall currents measured in DC and AC voltammetry in industrial conditions are the combination of currents from Cu^{2+} reduction to Cu^{+}, and Cu^{+} reduction to Cu metal. In conditions designed to slow charge transfer kinetics, these two reduction steps can be separately observed by ACV. The shapes of the harmonic current peaks for Cu^{+} reduction confirm previous reports that Cu^{+} reduction occurs as an adsorbed species. In industrial conditions, Fe^{2+} lowers the overall reaction kinetics measured in DC and AC voltammetry. ACV results show that Fe^{2+} has a stronger effect on Cu^{+} reduction, producing lower peak currents at larger overpotentials.

Chapter 7

Acknowledgements

The author would like to extend her thanks to her advisor, Professor Antoine Allanore, for his teaching, guidance, and mentorship throughout this research project. She would also like to thank members of the Allanore Research Group for their help and support, especially former postdoctoral associate Sangkwon Lee. The author would also like to thank Professors Tomás Vargas and Melanie Colet-Lagrille, and their research group, El Laboratorio de Hidrometalurgia y Electrometalurgia, in Universidad de Chile, in particular their students Claudia Aravena and Rodrigo Valenzuela, for their collaboration, research efforts, and support. The author would also like to acknowledge the MISTI-Chile program for its financial support throughout this project.

References

1. T. C. Liu, C. M. Liu, Y. S. Huang, C. Chen, and K. N. Tu, *Scr. Mater.*, **68**, 241–244 (2013) http://dx.doi.org/10.1016/j.scriptamat.2012.10.024.

2. Y. Liu et al., *IEEE Trans. Components Packag. Technol.*, **33**, 127–137 (2010).

3. F. Qiao, B. B. O'Brien, K. a. Dunn, and a. C. West, *J. Electrochem. Soc.*, **160**, D271–D278 (2013) http://jes.ecsdl.org/cgi/doi/10.1149/2.142306jes.

4. N. D. Nikolić, G. Branković, M. G. Pavlović, and K. I. Popov, *J. Electroanal. Chem.*, **621**, 13–21 (2008).

5. N. D. Nikolic, *ZAŠTITA Mater.*, **51** (2010).

6. P. Vargas, Tomás, Parra, in *International Copper Conference,*, p. 51 (2013).

7. Z. D. Stanković, V. Cvetkovski, and M. Vuković, *J. Min. Metall. Sect. B Metall.*, **44**, 107–114 http://www.doiserbia.nb.rs/Article.aspx?ID=1450-53390801107S#.VTpWua3BzGd.

8. M. A. Pasquale, L. M. Gassa, and A. J. Arvia, *Electrochim. Acta*, **53**, 5891–5904 (2008) http://www.sciencedirect.com/science/article/pii/S0013468608004799.

9. Z. D. Stanković, *J. Electrochem. Soc.*, **128**, 1862 (1981).

10. Z. D. Stanković, *Electrochim. Acta*, **29**, 407–409 (1984) http://www.sciencedirect.com/science/article/pii/0013468684870838.

11. J. O. Bockris and M. Enyo, *Trans. Faraday Soc.*, **58**, 1187 (1962) http://pubs.rsc.org/en/content/articlehtml/1962/tf/tf9625801187.

12. E. Mattsson and J. O. Bockris, *Trans. Faraday Soc.*, **55**, 1586 (1959).

13. T. Hurlen, G. Ottesen, and A. Staurset, *Electrochim. Acta*, **23**, 39–44 (1978) http://www.sciencedirect.com/science/article/pii/0013468678870315.

14. S. Venkatesh, *J. Electrochem. Soc.*, **128**, 2588 (1981).

15. J. L. Anderson and I. Shain, *Anal. Chem.*, **50**, 163–171 (1978) http://pubs.acs.org/doi/pdf/10.1021/ac50023a037.

16. J. L. Anderson and I. Shain, *Anal. Chem.*, **48**, 1274–1282 (1976) http://pubs.acs.org/doi/pdf/10.1021/ac50003a007.

17. L. M. C. Pinto, P. Quaino, E. Santos, and W. Schmickler, *Chemphyschem*, **15**, 132–8 (2014) http://www.ncbi.nlm.nih.gov/pubmed/24376128.

18. J. Vazquez-Arenas, *Electrochim. Acta*, **55**, 3550–3559 (2010) http://dx.doi.org/10.1016/j.electacta.2010.01.050.

19. A. A. Shaikh et al., *Int. J. Electrochem. Sci.*, **6**, 2333–2343 (2011) http://www.electrochemsci.org/papers/vol6/6072333.pdf.

20. D. E. Smith, in *Electroanalytical Chemistry: A Series of Advances (I)*, A. J. Bard, Editor, p. 1–155, Marcel Dekker, Inc., New York (1966).

21. A. M. Bond, N. W. Duffy, S.-X. Guo, J. Zhang, and D. Elton, *Anal. Chem.*, **77**, 186A–195A (2005).

22. A. a Sher et al., *Anal. Chem.*, **76**, 6214–28 (2004) http://www.ncbi.nlm.nih.gov/pubmed/15516112.

23. E. Mashkina et al., *J. Electroanal. Chem.*, **690**, 104–110 (2013) http://dx.doi.org/10.1016/j.jelechem.2012.11.002.

24. M. J. A. Shiddiky, A. P. O'Mullane, J. Zhang, L. D. Burke, and A. M. Bond, *Langmuir*, **27**, 10302–11 (2011) http://dx.doi.org/10.1021/la2017819.

25. W. H. Reinmuth, *Anal. Chem.*, **40**, 185–194 (1968).

26. J. W. Dini, *Electrodeposition - The Materials Science of Coatings and Substrates*, William Andrew Publishing/Noyes, (1993) http://app.knovel.com/web/toc.v/cid:kpETMSCS02/viewerType:toc/root_slug:electrodeposition-materials/b-off-set:0/b-cat-name:Adhesives, Coatings, Sealants %26 Inks/b-cat-slug:adhesives-coatings-sealants-inks/b-cat-id:217/b-off-set:0/b-order-by:name/b-sort-by:ascending/b-filter-by:all-content.

27. M. Paunovic and M. Schlesinger, in *Fundamentals of Electrochemical Deposition*,, p. 77–112, John Wiley & Sons, Inc. (2006).

28. A. J. Bard and L. R. Faulkner, *Electrochemical Methods- Fundamentals and Applications*, Second., J. Wiley, New York, (2001).

29. E. Budevski, G. Staikov, and W. J. Lorenz, *Electrochim. Acta*, **45**, 2559–2574 (2000) http://www.sciencedirect.com/science/article/pii/S0013468600003534.

30. D. R. Turner and G. R. Johnson, *J. Electrochem. Soc.*, **109**, 798–804 (1962).

31. L. W. Yip, thesis, University of Hong Kong (1983).

32. J. Fuentes-Aceituno and G. Lapidus, in *XI International Hydrogen Congress*,, p. 1–21 (2011) http://www.iie.org.mx:8080/SitioGENC/hydrogen2011/MemCongress/PROCEEDINGS/Hydrogen2011_Sub83.pdf.

List of Figures

List of Tables